JACS Au
AN OPEN ACCESS JOURNAL OF THE AMERICAN CHEMICAL SOCIETY

pubs.acs.org/jacsau Article

Multiple Promotional Effects of Vanadium Oxide on Boron Nitride for Oxidative Dehydrogenation of Propane

Xiao Jiang,[▽] Xuanyu Zhang,[▽] Stephen C. Purdy, Yang He, Zhennan Huang, Rui You, Zeyue Wei, Harry M. Meyer III, Jiuzhong Yang, Yang Pan, Peiwen Wu, Wenshuai Zhu, Miaofang Chi, Katharine Page, Weixin Huang,* and Zili Wu*

Cite This: *JACS Au* 2022, 2, 1096−1104 Read Online

ABSTRACT: Featuring high olefin selectivity, hexagonal boron nitride (h-BN) has emerged recently as an attractive catalyst for oxidative dehydrogenation of propane (ODHP). Herein, we report that dispersion of vanadium oxide onto BN facilitates the oxyfunctionalization of BN to generate more BO_x active sites to catalyze ODHP via the Eley−Rideal mechanism and concurrently produce nitric oxide to initiate additional gas-phase radical chemistry and to introduce redox VO_x sites to catalyze ODHP via the Mars−van Krevelen mechanism, all of which promote the catalytic performance of BN for ODHP. As a result, loading 0.5 wt % V onto BN has doubled the yield of light alkene (C_2−C_3) at 540−580 °C, and adding an appropriate concentration of NO in the reactants further enhances the catalytic performance. These results provide a potential strategy for developing efficient h-BN-based catalysts through coupling gas-phase and surface reactions for the ODHP process.

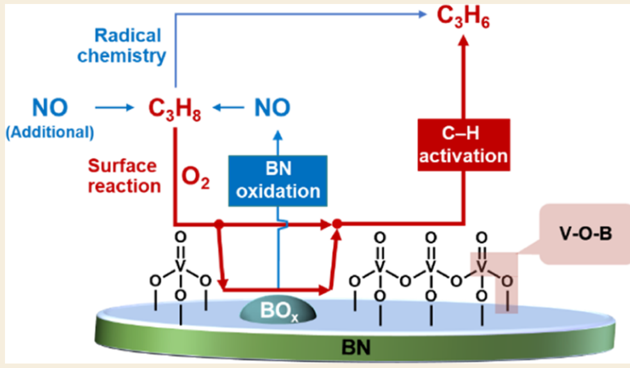

KEYWORDS: *oxidative dehydrogenation, hexagonal boron nitride, vanadium oxide, oxyfunctionalization, nitric oxide*

1. INTRODUCTION

Propylene (C_3H_6) is one of the important building blocks for a large number of chemicals in the petrochemical industry.[1] Technologies that have been widely implemented to produce propylene include petroleum-derived steam cracking and fluid catalytic cracking.[1] Direct dehydrogenation of propane (DHP) has emerged as an attractive approach, as evidenced in the Oleflex process (Honeywell, UOP), which features a higher propylene yield than other technologies.[1] However, the inherent endothermicity results in concomitant thermodynamic limitations and high energy input, as well as surface coking.[2] The oxygen-assisted oxidative dehydrogenation of propane (O_2-ODHP) provides alternatives to overcome these intrinsic issues, yet the overoxidation signifies the major research challenge for this reaction route.[3]

Redox-active metal oxides such as VO_x have been extensively studied for ODHP reaction, and the surface reaction typically proceeds via the Mars−van Krevelen (MvK) mechanism.[4−7] Hexagonal boron nitride (h-BN) has emerged as a breakthrough for the O_2-ODHP reaction because it features a high selectivity of light alkenes (i.e., ethylene and propylene) with negligible CO_x formation.[2,3,8−17] The reaction on boron-based catalysts is proposed to proceed through Eley−Rideal (ER) mechanism, in which the radical chemistry in the gas phase is proposed mostly through computational efforts in conjunction with the progress in oxidative coupling of methane reaction.[3,8,18−21] By examining the C_2/C_1 ratios in products, Wang and Lin have proposed the important role of methyl radicals in forming ethylene in the gas phase.[22] Our recent work directly observed the presence of methyl radicals in the gas phase during BN-catalyzed ODHP using the synchrotron photoionization mass spectroscopy technique.[19]

The proposed active sites include mixed amorphous mixed boron oxide/hydroxide $B(OH)_xO_{3-x}$ (x = 0−3)[13] and dihydroxyl boron-oxide species.[20] Due to the highly dynamic restructuring of boron species under reaction conditions, metastable boron species are also studied.[23,24] Thus, it is generally accepted that the oxidized B sites formed through the concurrent oxyfunctionalization of BN with gas-phase radical chemistry are the active sites for the ODHP reaction.[3,8] Very recently, plasma treatment was reported to regulate the local environment of h-BN by creating nitrogen defects, favoring the

Received: December 2, 2021
Revised: March 3, 2022
Accepted: March 24, 2022
Published: April 1, 2022

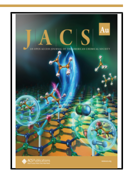

generation of BO_x active sites.[11] Efforts are also devoted to developing BO_x-containing advanced materials for ODHP reaction, including boron phosphate[25,26] and metal−organic framework-derived catalysts.[27]

Although the combination between VO_x and BN is known in the literature for propane oxidation to acrolein,[28] the role of VO_x in modifying the BN surface and its correlation with ODHP catalytic performance are elusive. In the present work, we hypothesize that the introduction of redox-active species such as VO_x could in situ tune the local chemical environment of BN by introducing oxyfunctional groups with its redox performance as in a typical supported VO_x system. Indeed, our results show that the redox-active VO_x additive can significantly enhance the catalytic performance of BN in ODHP. Characterized by Raman spectroscopy, X-ray photoelectron spectroscopy (XPS), X-ray absorption spectroscopy (XAS), scanning- ransmission electron microscopy (STEM), and synchrotron vacuum ultraviolet photoionization mass spectroscopy (SVUV-PIMS), the VO_x additive, on the one hand, contributes to catalyzing ODHP via the MvK mechanism; on the other hand, it is found to facilitate the oxyfunctionalization of BN to not only generate more BO_x active sites to catalyze ODHP via the ER mechanism but also produce NO to further induce gas-phase chemistry for enhanced ODHP.

2. EXPERIMENTAL SECTION

2.1. Preparation of Catalysts

2.1.1. h-BN with High Surface Area. h-BN was synthesized according to the procedure reported elsewhere[29] and is described briefly herein. The exfoliation was conducted in a muffle oven heated to 700 °C and maintained at this temperature, unless otherwise noted. 1 g of commercial h-BN (Sigma-Aldrich, 99%) was treated at 700 °C for 5 min. Then, the boron nitride was transferred to a 4 L Teflon beaker which contained 100 mL of liquid nitrogen, followed by covering with a lid. The treated boron nitride was carefully recollected after the liquid nitrogen was completely volatilized. The exfoliation procedure was repeated 10 times. Afterward, the obtained boron nitride was dispersed in H_2O and ultrasonicated for 10 min, followed by centrifugation at a speed of 1500 rpm to remove unexfoliated materials. The upper liquid was collected and dried at 70 °C overnight to obtain h-BN with a high surface area of 72.7 m^2 g^{-1}. The as-synthesized h-BN was pretreated under the reaction atmosphere ($C_3H_8/O_2/He$ = 1/1/38) at 500 °C for 4 h prior to further impregnation. The pretreated materials were denoted as BN-T throughout the paper, wherein the T represents "treated" samples.

2.1.2. VO_x/BN-T Catalyst. V-loaded BN-T catalysts were prepared by impregnation. A desired amount of V precursor, namely, NH_4VO_3, was dissolved in 2−3 mL of ultrapure H_2O at 80 °C, followed by adding BN-T (0.5 g) into the solution and stirring vigorously until water was volatilized. The mixture was dried at 100 °C overnight and calcined at 450 °C in static air for 4 h with a ramp rate of 2 °C min^{-1}. The catalysts were denoted as *x*V/BN-T, wherein *x* represents the mass-based V loading and ranges from 0 to 1.0 wt %.

2.1.3. BO_x/SiO_2, VO_x/SiO_2, and $VO_x/BO_x/SiO_2$ Catalysts. BO_x/SiO_2 catalysts were prepared by impregnation. A certain amount of H_3BO_3 was dissolved in 10 mL of ultrapure H_2O at 70 °C, followed by addition of 0.5 g of SiO_2. The mixture was vigorously stirred at 80 °C for 1 h and then dried in an oven at 100 °C overnight. Calcination was conducted at 450 °C in static air for 4 h with a ramp rate of 2 °C min^{-1}. The calcined catalysts were denoted as yBO_x/SiO_2, wherein y represents mass-based B loading and is fixed at 5 wt %. VO_x/SiO_2 catalysts were prepared following the same procedure as BO_x/SiO_2, and the V loading was fixed at 0.5 and 1.0 wt % for comparison. The VO_x-loaded BO_x/SiO_2 catalyst was prepared by a method similar to that of VO_x/BN-T, and the V loading was fixed at 1.0 wt %.

2.2. Catalytic Performance Evaluation

The activity test of the ODHP reaction was performed using an Altamira Instruments system (AMI-200). In a typical test, 100 mg of catalyst (60−80 mesh) was diluted with 300 mg of quartz sand (60−80 mesh). The mixture was loaded in a quartz U-tube (i.d. = 10 mm) with quartz wool at both ends of the mixture. Prior to the activity test, the catalyst bed was treated in the mixture of $C_3H_8/O_2/He$ (1/1/38) at 600 °C for 4 h with gas hourly space velocity (GHSV) = 18,000 mL g^{-1} h^{-1}, followed by oxidation in 5% O_2/He at 500 °C for 1 h under 30 mL min^{-1}. Then, the activity test was initiated by switching to the mixture reaction gas of $C_3H_8/O_2/He$ (1/1/38) with GHSV = 18,000 mL g^{-1} h^{-1}. The reaction was conducted in the temperature range of 480−600 °C with 20 °C as an interval. Each temperature was held for 2 h for data collection. For the NO-assisted O_2-ODHP reaction, 0.1% NO/He or 2% NO/Ar was introduced to alter the NO concentrations at 180, 250, 350, and 3500 ppm. GHSV was fixed at 24,000 mL g^{-1} h^{-1}, while the C_3H_8/O_2 ratio remained unchanged.

Kinetic studies were conducted after the initial treatment, as described above. Then, the temperature was decreased to the desired temperature (i.e., 540 °C), followed by switching to the reaction gas mixtures using the premixed cylinders 5% C_3H_8/He, 5% O_2/He, and Ar. The partial pressures of both C_3H_8 and O_2 were varied from ca. 0.4 to 2.5%. While exploring the effect of the C_3H_8 partial pressure, the partial pressure of O_2 was fixed at 2.5% and vice versa. Ar was introduced to keep the GHSV fixed at 24,000 mL g^{-1} h^{-1}. The reaction order was calculated by fitting the gas composition-dependent activity data to the power law in the logarithmic relationship,[3,30,31] while the apparent activation energy was calculated by using the Arrhenius equation.[3,19]

Compositions of products were analyzed periodically using an online SRI 8610C gas chromatograph equipped with both thermal conductivity detector (TCD) and flame ionization detector (FID). MTX-WAX and Molecular Sieve 5A columns were attached to the TCD, analyzing O_2, NO, CO, and CO_2, while HayeSep-D and alumina were attached to the FID, analyzing hydrocarbons including C_3H_8, C_3H_6, C_2H_6, C_2H_4, and CH_4. A mass spectrometer (Pfeiffer Vacuum) was also coupled with the gas chromatograph to monitor the real-time evolutions of reactants and products. The carbon balance was generally ca. 95%. The absence of mass and heat-transfer limitations were confirmed by the Weisz−Prater criterion and the Mears criterion. Detailed calculations are shown in the Supporting Information.

2.3. Characterization of Catalysts

Nitrogen (N_2) physisorption was performed using a Micromeritics Gemini 2375 surface area and pore size analyzer at −196 °C. The samples were degassed for 1 h prior to measurement. The Brunauer−Emmett−Teller method was used to calculate the surface areas.

Powder X-ray diffraction (XRD) patterns were recorded using a PANalytical X'Pert Pro system with Cu Kα radiation. Diffractograms were obtained at incident angles for 2θ = 5−65°.

Scanning electron microscopy (SEM) images were collected using a Zeiss Merlin system operated at 5.00 kV. STEM images were acquired through a JEOL NEOARM microscope operated at 80 kV.

Raman spectroscopy was performed on a multiwavelength Raman system using UV 244 nm laser excitation. Raman scattering was collected via a customized ellipsoidal mirror and directed by a fiber optics bundle to the spectrograph stage of a triple Raman spectrometer (Princeton Instruments Acton Trivista 555). An edge filter (Semrock) was used in front of the UV−vis fiber optic bundle (Princeton Instruments) to block the laser irradiation. A neutral density filter was used to attenuate the laser power to 20% so that the laser power at the sample position is less than 5 mW. A UV-enhanced liquid N_2-cooled CCD detector (Princeton Instrument) was employed for signal detection. The Raman catalytic reactor (Linkam CCR1000) was placed on an XY stage (Princeton Scientific, OptiScan XY system). During the acquisition, the stage translated in the raster mode, which could provide the information of heterogeneity of the samples. The fast translation and the attenuated laser power were also able to minimize the laser damage of the sample. For dehydrated

https://doi.org/10.1021/jacsau.1c00542
JACS Au 2022, 2, 1096−1104

spectra, the catalysts were treated in 2% O_2/He/Ar with a flow rate of 30 mL min^{-1} at 500 °C for 30 min, followed by cooling to 120 °C and acquiring the spectra after being stabilized for 30 min. During in situ Raman measurements, the dehydrated catalysts were sequentially exposed to 2% O_2/He/Ar and then to C_3H_8/O_2/He/Ar (C_3H_8/O_2 = 1/1) with a duration of 30 min for each at 550 °C.

XPS was performed using a Thermo Scientific (Waltham, MA, USA) model K-Alpha XPS instrument. The instrument utilizes monochromated, microfocused Al Kα X-ray (1486.6 eV) with a variable spot size (i.e., 30−400 μm). Analyses of the sample were performed with the 400 μm X-ray spot size for maximum signal to obtain an average surface composition over the largest possible area. The instrument has a hemispherical electron energy analyzer equipped with a 128-channel detector system. The base pressure in the analysis chamber was typically 2 × 10^{-9} mbar or lower. The samples were prepared for analysis by dispersing the powder material onto double-sided tape fixed to a clean glass slide. After transferring the samples into the analysis chamber, the survey spectra (pass energy = 200 eV) were acquired for each sample. Next, high-resolution core level spectra (pass energy = 50 eV) were acquired for a detailed chemical state analysis. All spectra were acquired with the charge neutralization flood gun (combination of low energy electrons and argon ions) turned on to maintain a stable analysis condition. The typical pressure in the analysis chamber with the flood gun operating was 2 × 10^{-7} mbar. Data were collected and processed using the Thermo Scientific Avantage XPS software package (v.5.96).

Detailed procedures of XAS and SVUV-PIMS are described in the Supporting Information.

3. RESULTS AND DISCUSSION

3.1. Activity Performance of VOx-Loaded h-BN Catalyts for ODHP Reaction

A series of VO_x-loaded BN-T catalysts were prepared by impregnation. The catalyst is denoted as xV/BN-T throughout the paper, wherein x represents the loading of vanadium in wt % (ranging from 0 to 1 wt %) and the "T" in BN-T indicates that the h-BN support was treated under C_3H_8/O_2 atmosphere prior to impregnation. The resultant activity performance of VO_x/BN-T catalysts is shown in Figure 1. All VO_x-loaded BN-T catalysts exhibit higher C_3H_8 conversion (Figure 1A) and light-alkene (C_2−$C_3^=$) yield (Figure 1B) than the benchmark BN-T under the same reaction conditions, especially for 0.5V/BN-T. At 540−580 °C, the light-alkene yield of 0.5V/BN-T is doubled compared to that of BN-T. The increase in the propylene yield on 0.5V/BN-T is also nearly doubled within the same temperature range (Figure S1A). The catalyst with the optimal V loading, namely, 0.5V/BN-T, presents good cyclability in three consecutive light-off tests (Figure S2). Noteworthily, the reaction conditions in the present work used diluted C_3H_8 compositions. To evaluate the stability and cyclability for practical purposes, further tests under high C_3H_8 compositions and long duration are warranted.

As shown in Figure 1C, the selectivity of propylene decreases with the increase in propane conversion for all catalysts (at high temperatures), while an inverted trend is observed for ethylene selectivity (Figure 1D). This is consistent with previous work, which demonstrates the increased contribution of gas-phase radical chemistry at higher temperatures in the formation of the secondary product ethylene.[3] V/BN-T catalysts present relatively lower C_3H_6 selectivity than BN-T at lower C_3H_8 conversions, the difference of which is particularly appreciable for 0.5V/BN-T (Figure 1C). Meanwhile, BN-T also outperforms the VO_x/BN-T catalysts in C_2H_4 selectivity (Figure 1D), resulting in the decreased net selectivity of light alkenes on VO_x/BN-T than

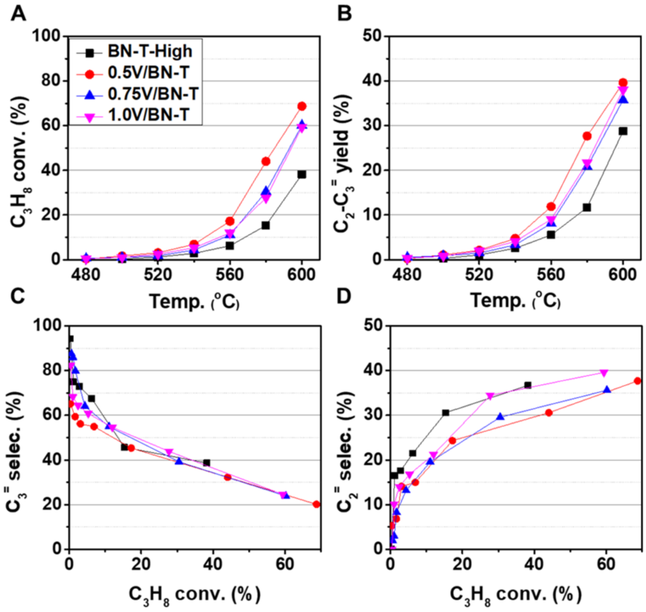

Figure 1. Temperature-dependent changes in C_3H_8 conversion (A), light-alkene (C_2−$C_3^=$) yield (B), and plotted light-alkene selectivity-C_3H_8 conversion relationship (C,D) on VO_x/BN-T catalysts for the O_2-ODHP reaction. Reaction conditions: C_3H_8/O_2/He (1/1/38) and GHSV = 18,000 mL g^{-1} h^{-1}.

that on BN-T at higher conversions (Figure S1B). As aforementioned, Wang and Lin have proposed the methyl radical-involved reaction paths in the gas phase, one of which is to produce C_2 products by the coupling reaction.[22] The presence of methyl radicals is then supported by the in situ SVUV-PIMS results.[19] Thus, the decreased C_2H_4 selectivity on V/BN-T is indicative of the interference from the VO_x-induced surface contribution.[4−7] Interestingly, the C_3H_6 selectivity of VO_x/BN-T tends to coincide with that of BN-T at higher conversions. This implicates that VO_x plays a role in propane dehydrogenation on the surface at lower conversions, while the characteristic gas-phase contribution of BN dominates at higher conversion.

To understand the role of VO_x, BO_x, and BN in the ODHP reaction, we performed two arrays of control experiments, including the comparison between 0.5V/SiO_2, BN-T, and the physical mixture of 0.5V/SiO_2 and BN-T, as well as the comparison between 1V/SiO_2, 5B/SiO_2, the physical mixture of 1V/SiO_2 and 5B/SiO_2, and 1V/5B/SiO_2 (prepared by sequential impregnations). Figure S3 shows the results through the comparison between 0.5V/SiO_2, BN-T, their physical mixture, and 0.5V/BN-T. In general, in comparison to BN-T, the physical mixture of 0.5V/SiO_2 and BN-T exhibits similar trends in activity and selectivity to 0.5V/BN-T, in which a slight increase in C_3H_8 conversion and decreases in C_3H_6 and C_2H_4 selectivities are evident. In particular, the physical mixture presents moderate C_2H_4 selectivity between BN-T and 0.5V/SiO_2. This indicates that the presence of BN-T contributes to the C_2H_4 formation through the gas-phase reactions, therefore leading to an increase in C_2H_4 selectivity in comparison to 0.5V/SiO_2 alone.[19,22] Meanwhile, VO_x induces the surface reaction, resulting in a reduction in C_2H_4 selectivity in comparison to BN-T.[4,8] These observations are consistent with those on V/BN-T catalysts, corroborating the contributions from both surface and gas-phase reactions with the combination of VO_x and BN. Notably, the enhancement of

https://doi.org/10.1021/jacsau.1c00542
JACS Au 2022, 2, 1096−1104

activity on 0.5V/BN-T significantly surpasses that on the physical mixture (Figure S3A,B). This demonstrates better synergism by loading a certain density of VO_x directly onto BN. By contrast, such an enhancement is not evident from the other array of control experiments on $1V/SiO_2$, $5B/SiO_2$, and their physical mixture (Figure S4). Nor is it observed on $1V/5B/SiO_2$. Besides, the physical mixture only exhibits a slightly higher selectivity toward C_2H_4 than $1V/SiO_2$ under isoconversional conditions (Figure S4D), which is, however, much lower than $5B/SiO_2$ or $1V/5B/SiO_2$. In conjunction with the observed promoting effect on V/BN-T, such a contrast between these two arrays of control experiments implies that the presence of VO_x on BN-T not only contributes to the ODHP reaction but may also tune the BN-T surface with positive impacts, such as oxyfunctionalization. This will be studied by XAS and XPS and is discussed in Section 3.2.

For V/BN-T catalysts, the apparent activation energy (E_{app}) decreases with the increase in V loadings (i.e., ca. 250 to 200 kJ mol^{-1}, Figure 2A), indicative of the surface contribution of

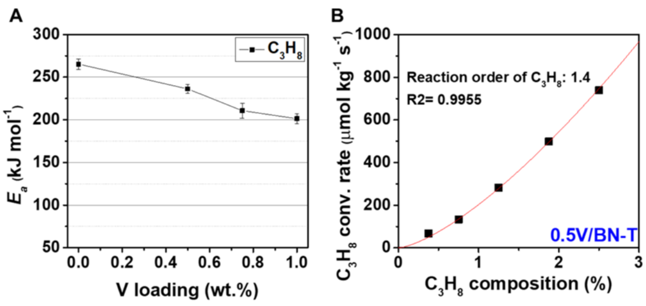

Figure 2. (A) Variations of apparent activation energy (E_a) as a function of V loadings and (B) effect of C_3H_8 composition % on the C_3H_8 conversion rate on 0.5V/BN-T at 540 °C. Reaction conditions in (A): $C_3H_8/O_2/He$ (1/1/38), GHSV = 18,000 mL g^{-1} h^{-1}, and C_3H_8 conv. <15%. Reaction conditions in (B): 0.4–2.5% C_3H_8/2.5% O_2, balanced in He and Ar and GHSV = 24,000 mL g^{-1} h^{-1} (see Figure S6 for the effect of O_2 composition % on the C_3H_8 conversion rate).

added VO_x in the observed synergism on improved activity. This is also corroborated by the results of kinetic studies at different C_3H_8 partial pressures, in which the propane consumption rate is 1.4-order dependent on the propane partial pressure in the presence of VO_x (Figure 2B), lower than the 1.8-order on the BN support alone (Figure S5) and the reported second-order dependence on other BN alone.[3] Noteworthily, the lowest E_{app} attained on 1.0V/BN-T is still higher than those reported for supported VO_x catalysts for O_2-ODHP (i.e., 80–170 kJ mol^{-1}).[6] Clearly, the ER mechanism, proposed for BN catalysts, still dominates despite the presence of VO_x.

3.2. Characterization of Catalyst Structures

To study the catalyst structure, especially the interaction between surface BO_x/BN and VO_x species, and its correlation with the enhanced ODHP activity, the VO_x/BN-T catalysts were characterized by various techniques. The SEM images of VO_x/BN-T show a morphology similar to those of fresh BN and BN-T (Figure S7). Diffraction peaks of BN phases dominate the XRD patterns for VO_x/BN-T catalysts (Figure S8). No clear diffraction peaks are evident for VO_x phases when the V loading is below 1.0 wt %. This suggests the formation of either highly dispersed (nanocrystalline) or amorphous V-containing species. Due to the nanostructured/amorphous nature and lower V loadings, XRD is not suitable to provide structural information of VO_x.

The same catalysts were then characterized by Raman spectroscopy (see Figure S9 for BN and BN-T). The characteristic G band of BN, namely, the interlayer Raman active E_{2g} mode, is observed at 1370.8 cm^{-1} for fresh BN, while the band slightly red shifts to 1369.8 cm^{-1} for 0.75V/BN-T, implying the VO_x-induced localized fixation effect on reduced in-plane strain (Figure S10).[32] Figure 3A shows the Raman

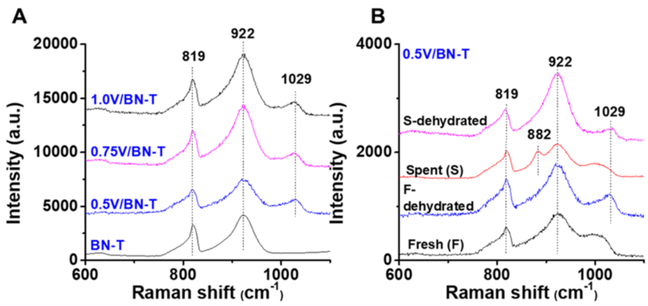

Figure 3. Raman (244 nm excitation) spectra of dehydrated VO_x/BN-T (A) and 0.5V/BN-T (B) under different conditions. Dehydration conditions: 2% O_2/He/Ar, 30 mL min^{-1}, 500 °C, and 30 min. The spent catalyst was collected after the ODHP activity test.

spectra of dehydrated VO_x/BN-T catalysts. The two peaks, centered at 819 and 922 cm^{-1}, are not due to any fundamental modes of h-BN but have been observed in previous studies with UV Raman.[33] Their assignment has not been fully resolved. Since the two bands are quite stable throughout our various experiments, they are not considered relevant to the ODHP reaction, so we focus rather on the surface vanadia species. For dehydrated catalysts, a band is observed at 1029 cm^{-1} for all VO_x/BN-T samples, signifying polyvanadate on the BN surface.[7,34] No sign of the crystalline V_2O_5 is observed at ca. 997 cm^{-1},[7,34] demonstrating that the VO_x is less than a monolayer coverage for all VO_x/BN-T catalysts. The Raman spectrum of the spent 0.5V/BN-T, collected after the O_2-ODHP reaction, shows a new band at 882 cm^{-1} (Figure 3B), which can be attributed to the borate species with hydroxylated non-ring boron (B-OH).[35] For comparison, BO_x/SiO_2 and $VO_x/BO_x/SiO_2$ have been prepared as benchmarks, and similar peaks are also evidenced (see Figure S11 for details). This band disappears after the dehydration, and the V═O stretch appears at a similar shift as seen in the fresh and dehydrated sample, indicating the integrity of the VO_x species during the ODHP.

The structure of VO_x species is confirmed by high-angle annular dark-field STEM (HAADF-STEM) analysis, which clearly evidences the presence of VO_x nanoclusters (polyvanadates) in Figure 4. Meanwhile, some single atoms are also observed from the HAADF images, indicating the presence of a small portion of monovanadate. To our knowledge, this is one of a few cases of coupled spectroscopy and microscopy in identifying the nature of VO_x in powder samples, thanks to the 2D nature of BN and high contrast in STEM.

Figure 5A shows the normalized pre-edge peak of the vanadium K edge XANES (X-ray absorption near edge structure) for 1.0VO_x/BN-T catalysts under different in situ treatments, along with those of reference compounds. Two sets of in situ measurements were performed on fresh 1.0V/BN-T.

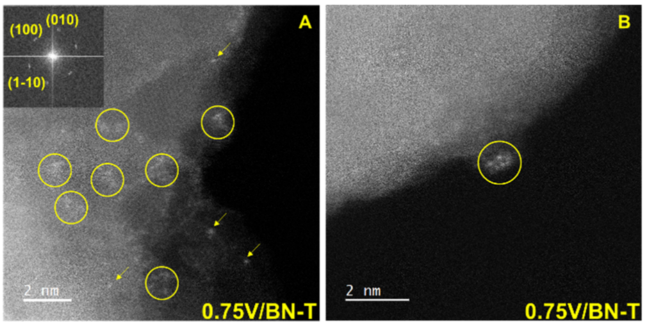

Figure 4. HAADF images of 0.75V/BN-T in different regions, along with the fast Fourier transform images of the BN substrate in the inset of (A). The arrows and circles highlight the surface monovanadate and polyvanadate, respectively.

The first measurement, comprising consecutive treatments in O_2, C_3H_8, and O_2 regeneration at 500 °C, was done to verify the reversible redox cycles of VO_x under reaction conditions. The catalyst treated in C_3H_8 presents a strong decrease in the intensity of the pre-edge peak and a shift toward lower photon energy, implying a partial reduction in the oxidation state and corresponding changes in the point group symmetry of vanadium in the catalyst (Figure 5A). Subsequent O_2 regeneration enables the recovery of the oxidation state of vanadium, as evidenced from the match between the initially O_2-treated and O_2-regenerated XANES. Clearly, VO_x can undergo redox cycling under our reaction conditions. To quantify the oxidation state and understand the local symmetry around vanadium, the normalized pre-edge peak area was plotted as a function of the pre-edge peak centroid. This method of XANES analysis has been widely used for the identification of unknown compounds in 3d metals.[36,37] The catalysts fall in a region bounded by V^{5+} and V^{4+} compounds, which is shown in Figure 5B. The O_2-treated catalyst, the O_2-regenerated catalyst, and the catalyst treated in C_3H_8/O_2 are all very similar in oxidation state and symmetry. After regeneration, the pre-edge peak shifts up in area and down in energy position, closer to that of NH_4VO_3 (T_d V^{5+}). This would be consistent with a small increase in the fraction of vanadium with tetrahedral coordination. This could be caused by the formation and dispersion of polyvanadate on the surface of BN-T or on BO_x formed via oxyfunctionalization. The absence of inactive crystalline phase V_2O_5 is also confirmed from the XANES results. These observations agree with the Raman results.

The second measurement includes exposing the same fresh catalyst in a mixture of C_3H_8/O_2 at 500 °C in an effort to determine the predominant oxidation state of vanadium under steady-state reaction conditions. As shown in Figure 6A, the catalysts treated in O_2 and C_3H_8/O_2 present almost overlapping XANES spectra, demonstrating that a majority of V stays in +5 under reaction conditions. This is also corroborated by the similar normalized pre-edge intensity versus pre-edge centroid energy, in which the pre-edge peak area and centroid are, within error, the same as that of the O_2-treated catalyst (Figure 6B).

For the coordination environment, the Fourier-transformed $k^3\chi(k)$ (extended X-ray absorption fine structure) of fresh 1.0V/BN-T, treated in situ in C_3H_8 and O_2, shows a nearest neighbor-peak position consistent with oxygen, indicating the V−O bond of the first shell of 1.0V/BN-T (Figure S14). Combined with the spectra of pre-edge XANES, the formation of VB_2 structure can be excluded under reaction conditions. Instead, VO_x species are anchored at the surface through the B−O−V bond. In sum, vanadium is present mostly as V^{5+} under reaction conditions, while the redox cycles of VO_x still occur with a rapid kinetics. In other words, VO_x contributes to the ODHP reaction via MvK mechanism with redox cycles.

To explore the effect of VO_x on the gas-phase radical chemistry, the gas-phase components from ODHP over 1.0V/BN-T and the support BN-T were analyzed online by SVUV-PIMS, and the results are shown in Figure 7. On BN-T, the methyl radical ($CH_3^\bullet$), with the m/z value at 15.03, is observed, demonstrating the contribution of gas-phase radical chemistry in attaining such a high selectivity toward light alkenes (Figure 7A).[19] As shown in Figure 7B, adding VO_x leads to a notable relative increase in NO and a relative reduction in $CH_3^\bullet$ and C_2H_4. It is likely that the presence of VO_x boosts the surface reaction, and the formation of the B−O−V structure tunes the local environment of the active sites B-OH, thereby perturbing the gas-phase radical chemistry. Interestingly, the increase in NO in the gas phase is indicative of the NO release from the

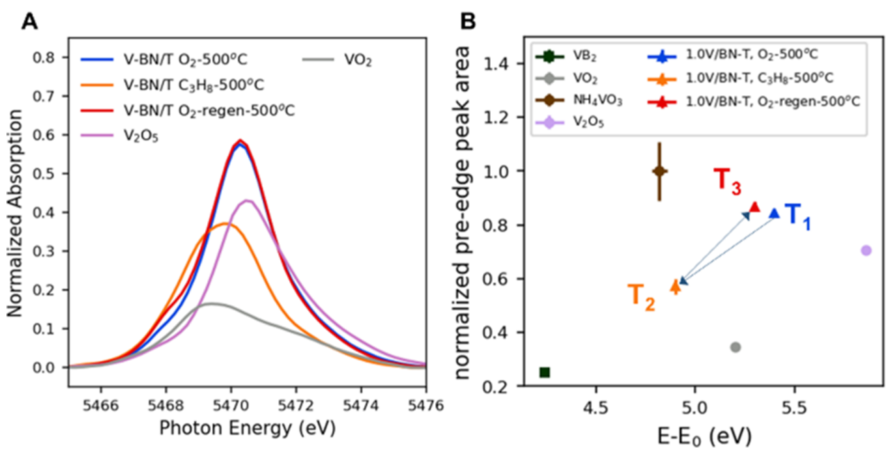

Figure 5. Background-subtracted XANES spectra of vanadium pre-edge peaks for 1.0V/BN-T after consecutive treatments in O_2, C_3H_8, and O_2 regeneration (A) and corresponding normalized pre-edge intensity vs pre-edge centroid energy relative to the threshold energy of V metal (5465 eV) for 1.0V/BN-T under different treatments and for reference compounds (B). Spectra of reference compounds, as well as detailed data analysis and discussion, can be found in the Supporting Information (Tables S1, S2 and Figures S12, S13).

https://doi.org/10.1021/jacsau.1c00542
JACS Au 2022, 2, 1096−1104

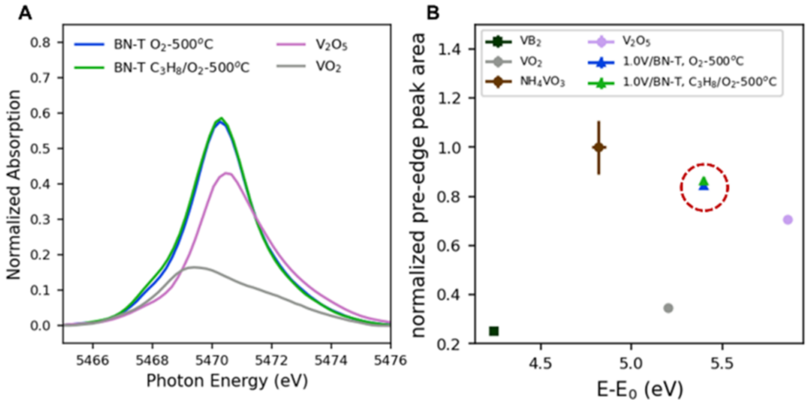

Figure 6. Background-subtracted XANES spectra of vanadium pre-edge peaks for 1.0V/BN-T after the single treatment in C_3H_8/O_2 as well as that after O_2 treatment as reference (A) and corresponding normalized pre-edge intensity vs pre-edge centroid energy relative to the threshold energy of V metal (5465 eV) for 1.0V/BN-T and for reference compounds (B). Spectra of reference compounds, as well as detailed data analysis and discussion. can be found in the Supporting Information (Tables S1, S2 and Figures S12, S13).

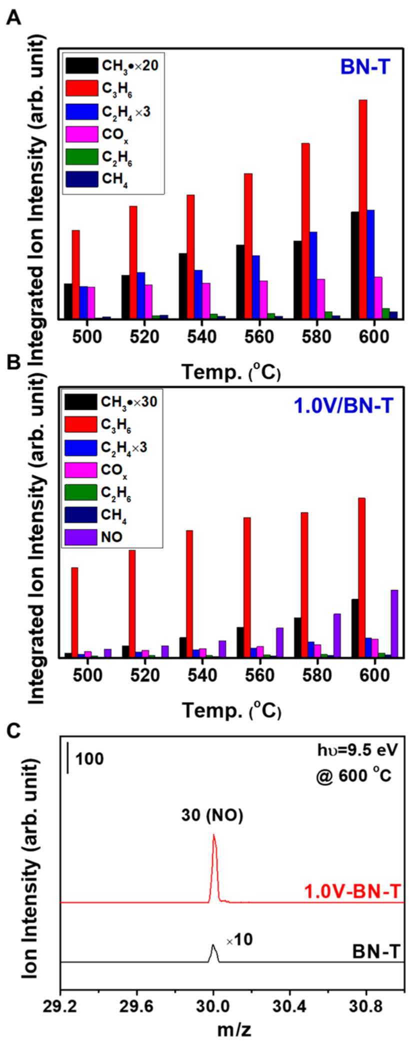

Figure 7. Integrated ion intensities of various components in the gas phase of O_2-ODHP reaction over BN-T (A) and 1.0V/BN-T (B) at 600 °C. (C) SVUV-PIMS spectra of the gas-phase NO for ODPH reaction at 600 °C on BN-T and 1.0V/BN-T. Photon energy = 9.5 eV. Note that only a trace amount of NO was detected for BN-T at 600 °C, so that it is not included in (A).

surface occurring concurrently with the reaction. Such a peculiar phenomenon can be associated with the dispersed VO_x species at the surface that facilitate the oxyfunctionalization of BN. In contrast, NO is barely observed from the SVUV-PIMS spectrum on BN-T in the gas phase, except a trace amount at 600 °C (Figure 7C). The blank test (Figure S15) shows no evident signals of gas-phase methyl radicals (m/z = 15) in the absence of a catalyst at 600 °C, nor does the control test present any NO (m/z = 30) signals in the presence of a catalyst at room temperature. This implies that all detected species in the gas phase on both BN-T and 1.0V/BN-T under ODHP reaction conditions are derived from the catalyst.

Early work has reported the positive role of NO in the gas-phase reaction in the partial oxidation of methane to oxygenates[38,39] and ODHP reaction via both homo- and heterogeneous catalysis.[40] The evolved NO in the gas phase inspires us to perform additional activity tests of ODHP reaction in the presence of various NO concentrations. As expected, such a NO-induced enhancement in activity is evidenced with the additional NO concentration below 350 ppm. The selectivity is also slightly increased. An excess addition such as 3500 ppm is detrimental (Figures S16 and S17). Similar NO concentration-dependent trends are also evidenced on SiO_2-supported BO_x catalysts (Figure S18). Of note, although the NO evolution is evidenced, it does not necessarily imply that this restructuring procedure of BN is continuous until all nitrogen species are stripped out. The light-off tests show the repeatability of 0.5V/BN-T for three consecutive tests under the present reaction conditions, demonstrating that VO_x plays an important role in the observed enhancement in activity (Figure S2).

To further verify the VO_x-facilitated oxyfunctionalization, XPS measurements were conducted on both fresh and spent BN-T and 0.75V/BN-T. Figure 8A shows the XP spectra of all samples in the region of B 1s. The major peak, centered at 190.8 eV, corresponds to B−N species on a flat surface for all samples.[11,41] Further deconvolution analysis reveals the other two B-containing surface species for fresh and spent BN and fresh 0.75V/BN-T, and they are B−O and BO_x centered at 191.3 and 192.2 eV, respectively.[9,41] For spent 0.75V/BN-T, the peak intensity of BO_x increases notably; moreover, a new peak emerges at 193.5 eV corresponding to B_2O_3 species at the surface.[41,42] Of note, the peak of B−O species is absent for the spent catalyst, which might be associated with the restructuring

https://doi.org/10.1021/jacsau.1c00542
JACS Au 2022, 2, 1096−1104

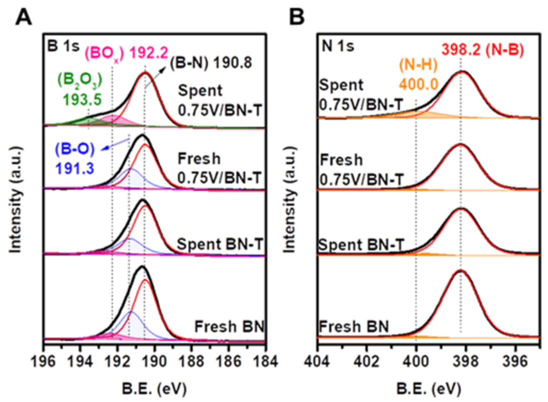

Figure 8. XP spectra of fresh and spent BN-T and 0.75V/BN-T catalysts in the regions of B 1s (A) and N 1s (B).

of the BN surface with the assistance of VO_x under the reaction conditions. Due to the formation of more BO_x species, a blueshift of O 1s peak for this spent 0.75V/BN-T is evidenced, signifying the substitution of nitrogen with oxygen at the BN surface (Figure S19).[14] Clearly, the presence of VO_x is conducive to forming BO_x species via oxyfunctionalization under reaction conditions, in line with the observation by the evolved NO from SVUV-PIMS. This can also be corroborated from the quantification analysis, as evidenced from the distinct higher oxygen and BO_x compositions in the spent samples (Tables 1 and S3). The major band at 398.2 eV in N 1s XP spectra is the nitrogen bonded with boron in BN at the surface (Figure 7B).[11] A subpeak at 400.0 eV corresponds to N−H species, implying the formation of N defects,[9] and these N−H species maximize at spent 0.75V/BN-T (Table S4). Recently, Lu et al. have reported that these N defects might lead to the evolution of active BO_x species.[11] Clearly, combined with the observations in this work, adding VO_x enables the tuning of the local chemical environment by facilitating the BN oxyfunctionalization to BO_x, along with the release of NO into the gas phase.

Table 1. Surface Composition of B-containing Species by XPS Analysis for Fresh and Spent BN-T and 0.75V/BN-T

	surface composition/at. %			
catalyst	B−N	B−O	BO_x	B_2O_3
fresh BN-T	29.7	13.5	2.5	
spent BN-T[a]	27.7	8.4	1.7	
fresh 0.75V/BN-T	26.1	11.5	1.3	
spent 0.75V/BN-T[a]	34.5		6.5	4.2

[a]Spent catalysts were collected after 12 h ODHP activity test at 600 °C.

4. CONCLUSIONS

In summary, a significant enhancement of light-alkene yield in ODHP is achieved through the synergism between VO_x and BN. The VO_x-induced increase in activity can be attributed to the well-dispersed VO_x species anchored at the surface as mono- and polyvanadate via B−O−V structure, which facilitates the surface oxyfunctionalization and exposes more BO_x for C−H activation. Meanwhile, NO is released during the facilitated oxyfunctionalization of BN, which also contributes to the rise in activity via mediating the gas-phase radical chemistry. In addition to the above roles, VO_x catalyzes the reaction via the redox cycles on the surface. Adding additional NO into the feed gas leads to further enhancement in the activity. While the quantification of the contribution from gas-phase and surface reactions is challenging and warrants further investigations, our findings shed light on developing efficient boron-based catalysts for the ODHP reaction by manipulating the interplay between homogenous gas-phase catalysis and heterogeneous surface catalysis.

ASSOCIATED CONTENT

Supporting Information

The Supporting Information is available free of charge at https://pubs.acs.org/doi/10.1021/jacsau.1c00542.

Materials used for catalyst preparation; calculations of mass and heat transfer; additional activity and kinetic results for O_2-ODHP reaction over V/BN-T and benchmarks; complementary characterization results including SEM, XRD, and Raman; detailed data analysis of XAS results; SVUV-PIMS results; activity results of NO-assisted O_2-ODHP reaction over V/BN-T and SiO_2-supported BO_x and VO_x/BO_x catalysts; and XPS results (PDF)

AUTHOR INFORMATION

Corresponding Authors

Weixin Huang − *Hefei National Laboratory for Physical Sciences at the Microscale, Key Laboratory of Surface and Interface Chemistry and Energy Catalysis of Anhui Higher Education Institutes, CAS Key Laboratory of Materials for Energy Conversion and Department of Chemical Physics, University of Science and Technology of China, Hefei 230026, P. R. China;* orcid.org/0000-0002-5025-3124; Email: huangwx@ustc.edu.cn

Zili Wu − *Chemical Sciences Division, Oak Ridge National Laboratory, Oak Ridge, Tennessee 37831, United States; Center for Nanophase Materials Sciences, Oak Ridge National Laboratory, Oak Ridge, Tennessee 37831, United States;* orcid.org/0000-0002-4468-3240; Email: wuz1@ornl.gov

Authors

Xiao Jiang − *Chemical Sciences Division, Oak Ridge National Laboratory, Oak Ridge, Tennessee 37831, United States;* orcid.org/0000-0002-4902-1828

Xuanyu Zhang − *Chemical Sciences Division, Oak Ridge National Laboratory, Oak Ridge, Tennessee 37831, United States; Hefei National Laboratory for Physical Sciences at the Microscale, Key Laboratory of Surface and Interface Chemistry and Energy Catalysis of Anhui Higher Education Institutes, CAS Key Laboratory of Materials for Energy Conversion and Department of Chemical Physics, University of Science and Technology of China, Hefei 230026, P. R. China*

Stephen C. Purdy − *Neutron Scattering Division, Oak Ridge National Laboratory, Oak Ridge, Tennessee 37831, United States;* orcid.org/0000-0002-9870-1029

Yang He − *Chemical Sciences Division, Oak Ridge National Laboratory, Oak Ridge, Tennessee 37831, United States*

Zhennan Huang − *Center for Nanophase Materials Sciences, Oak Ridge National Laboratory, Oak Ridge, Tennessee 37831, United States*

Rui You – *Hefei National Laboratory for Physical Sciences at the Microscale, Key Laboratory of Surface and Interface Chemistry and Energy Catalysis of Anhui Higher Education Institutes, CAS Key Laboratory of Materials for Energy Conversion and Department of Chemical Physics, University of Science and Technology of China, Hefei 230026, P. R. China*

Zeyue Wei – *Hefei National Laboratory for Physical Sciences at the Microscale, Key Laboratory of Surface and Interface Chemistry and Energy Catalysis of Anhui Higher Education Institutes, CAS Key Laboratory of Materials for Energy Conversion and Department of Chemical Physics, University of Science and Technology of China, Hefei 230026, P. R. China*

Harry M. Meyer III – *Chemical Sciences Division, Oak Ridge National Laboratory, Oak Ridge, Tennessee 37831, United States*

Jiuzhong Yang – *National Synchrotron Radiation Laboratory, University of Science and Technology of China, Hefei 230026, P.R. China;* orcid.org/0000-0002-7076-3412

Yang Pan – *National Synchrotron Radiation Laboratory, University of Science and Technology of China, Hefei 230026, P.R. China;* orcid.org/0000-0002-9360-3809

Peiwen Wu – *School of Chemistry and Chemical Engineering, Jiang Su University, Zhenjiang 212013, P. R. China;* orcid.org/0000-0002-4086-4706

Wenshuai Zhu – *School of Chemistry and Chemical Engineering, Jiang Su University, Zhenjiang 212013, P. R. China;* orcid.org/0000-0003-1265-4709

Miaofang Chi – *Center for Nanophase Materials Sciences, Oak Ridge National Laboratory, Oak Ridge, Tennessee 37831, United States;* orcid.org/0000-0003-0764-1567

Katharine Page – *Neutron Scattering Division, Oak Ridge National Laboratory, Oak Ridge, Tennessee 37831, United States; Department of Materials Science and Engineering, University of Tennessee, Knoxville, Tennessee 37996, United States;* orcid.org/0000-0002-9071-3383

Complete contact information is available at: https://pubs.acs.org/10.1021/jacsau.1c00542

Author Contributions

$^{\nabla}$X.J. and X.Z. contributed equally to this work.

Notes

The authors declare no competing financial interest.

ACKNOWLEDGMENTS

This work was supported as part of the Center for Understanding and Control of Acid Gas-Induced Evolution of Materials for Energy (UNCAGE ME), an Energy Frontier Research Center funded by the U.S. Department of Energy, Office of Science, Basic Energy Sciences under award # DE-SC0012577. Part of the work including the synthesis, activity test, and characterization (in situ Raman Spectroscopy and STEM) was done at the Center for Nanophase Materials Sciences, which is a DOE Office of Science User Facility. W.H. acknowledges the financial support of the National Natural Science Foundation of China (grant #91745202) and the Chinese Academy of Sciences and University of Science and Technology of China (grant #KY2060000176). XAS measurements were performed at the MRCAT bending magnet beamline of the Advanced Photon Source, Argonne National Laboratory. MRCAT operations are supported by the Department of Energy and the MRCAT member institutions. This research used resources of the Advanced Photon Source, a U.S. Department of Energy (DOE) Office of Science User Facility operated for the DOE Offices of Science by Argonne National Laboratory under contract no. DE-AC02-06CH11357.

REFERENCES

(1) Sattler, J. J. H. B.; Ruiz-Martinez, J.; Santillan-Jimenez, E.; Weckhuysen, B. M. Catalytic Dehydrogenation of Light Alkanes on Metals and Metal Oxides. *Chem. Rev.* **2014**, *114*, 10613–10653.

(2) Chen, S.; Chang, X.; Sun, G.; Zhang, T.; Xu, Y.; Wang, Y.; Pei, C.; Gong, J. Propane Dehydrogenation: Catalyst Development, New Chemistry, and Emerging Technologies. *Chem. Soc. Rev.* **2021**, *50*, 3315–3354.

(3) Grant, J. T.; Carrero, C. A.; Goeltl, F.; Venegas, J.; Mueller, P.; Burt, S. P.; Specht, S. E.; McDermott, W. P.; Chieregato, A.; Hermans, I. Selective Oxidative Dehydrogenation of Propane to Propene Using Boron Nitride Catalysts. *Science* **2016**, *354*, 1570–1573.

(4) Argyle, M. D.; Chen, K.; Bell, A. T.; Iglesia, E. Effect of Catalyst Structure on Oxidative Dehydrogenation of Ethane and Propane on Alumina-Supported Vanadia. *J. Catal.* **2002**, *208*, 139–149.

(5) Chen, K.; Bell, A. T.; Iglesia, E. Kinetics and Mechanism of Oxidative Dehydrogenation of Propane on Vanadium Molybdenum, and Tungsten Oxides. *J. Phys. Chem. B* **2000**, *104*, 1292–1299.

(6) Carrero, C. A.; Schloegl, R.; Wachs, I. E.; Schomaecker, R. Critical Literature Review of the Kinetics for the Oxidative Dehydrogenation of Propane over Well-Defined Supported Vanadium Oxide Catalysts. *ACS Catal.* **2014**, *4*, 3357–3380.

(7) Wu, Z.; Kim, H.-S.; Stair, P. C.; Rugmini, S.; Jackson, S. D. On the Structure of Vanadium Oxide Supported on Aluminas: UV and Visible Raman Spectroscopy, UV-Visible Diffuse Reflectance Spectroscopy, and Temperature-Programmed Reduction Studies. *J. Phys. Chem. B* **2005**, *109*, 2793–2800.

(8) Venegas, J. M.; Zhang, Z.; Agbi, T. O.; McDermott, W. P.; Alexandrova, A.; Hermans, I. Why Boron Nitride is such a Selective Catalyst for the Oxidative Dehydrogenation of Propane. *Angew. Chem., Int. Ed.* **2020**, *59*, 16527–16535.

(9) Mark, L. O.; Dorn, R. W.; McDermott, W. P.; Agbi, T. O.; Altvater, N. R.; Jansen, J.; Lebrón-Rodríguez, E. A.; Cendejas, M. C.; Rossini, A. J.; Hermans, I. Highly Selective Carbon-Supported Boron for Oxidative Dehydrogenation of Propane. *ChemCatChem* **2021**, *13*, 3611–3618.

(10) Shi, L.; Wang, Y.; Yan, B.; Song, W.; Shao, D.; Lu, A.-H. Progress in Selective Oxidative Dehydrogenation of Light Alkanes to Olefins Promoted by Boron Nitride Catalysts. *Chem. Commun.* **2018**, *54*, 10936–10946.

(11) Liu, Z.; Yan, B.; Meng, S.; Liu, R.; Lu, W. D.; Sheng, J.; Yi, Y.; Lu, A. H. Plasma Tuning Local Environment of Hexagonal Boron Nitride for Oxidative Dehydrogenation of Propane. *Angew. Chem., Int. Ed.* **2021**, *60*, 19691–19695.

(12) Grant, J. T.; McDermott, W. P.; Venegas, J. M.; Burt, S. P.; Micka, J.; Phivilay, S. P.; Carrero, C. A.; Hermans, I. Boron and Boron-Containing Catalysts for the Oxidative Dehydrogenation of Propane. *ChemCatChem* **2017**, *9*, 3623–3626.

(13) Love, A. M.; Thomas, B.; Specht, S. E.; Hanrahan, M. P.; Venegas, J. M.; Burt, S. P.; Grant, J. T.; Cendejas, M. C.; McDermott, W. P.; Rossini, A. J.; Hermans, I. Probing the Transformation of Boron Nitride Catalysts under Oxidative Dehydrogenation Conditions. *J. Am. Chem. Soc.* **2019**, *141*, 182–190.

(14) Shi, L.; Yan, B.; Shao, D.; Jiang, F.; Wang, D.; Lu, A.-H. Selective Oxidative Dehydrogenation of Ethane to Ethylene over A Hydroxylated Boron Nitride Catalyst. *Chin. J. Catal.* **2017**, *38*, 389–395.

(15) Zhou, Y.; Lin, J.; Li, L.; Pan, X.; Sun, X.; Wang, X. Enhanced Performance of Boron Nitride Catalysts with Induction Period for the

Oxidative Dehydrogenation of Ethane to Ethylene. *J. Catal.* **2018**, *365*, 14−23.
(16) Sheng, J.; Yan, B.; Lu, W.-D.; Qiu, B.; Gao, X.-Q.; Wang, D.; Lu, A.-H. Oxidative Dehydrogenation of Light Alkanes to Olefins on Metal-Free Catalysts. *Chem. Soc. Rev.* **2021**, *50*, 1438−1468.
(17) Venegas, J. M.; McDermott, W. P.; Hermans, I. Serendipity in Catalysis Research: Boron-Based Materials for Alkane Oxidative Dehydrogenation. *Acc. Chem. Res.* **2018**, *51*, 2556−2564.
(18) Kraus, P.; Lindstedt, R. P. It's a Gas: Oxidative Dehydrogenation of Propane over Boron Nitride Catalysts. *J. Phys. Chem. C* **2021**, *125*, 5623−5634.
(19) Zhang, X.; You, R.; Wei, Z.; Jiang, X.; Yang, J.; Pan, Y.; Wu, P.; Jia, Q.; Bao, Z.; Bai, L.; Jin, M.; Sumpter, B.; Fung, V.; Huang, W.; Wu, Z. Radical Chemistry and Reaction Mechanisms of Propane Oxidative Dehydrogenation over Hexagonal Boron Nitride Catalysts. *Angew. Chem., Int. Ed.* **2020**, *59*, 8042−8046.
(20) Zhou, H.; Yi, X.; Hui, Y.; Wang, L.; Chen, W.; Qin, Y.; Wang, M.; Ma, J.; Chu, X.; Wang, Y.; Hong, X.; Chen, Z.; Meng, X.; Wang, H.; Zhu, Q.; Song, L.; Zheng, A.; Xiao, F.-S. Isolated Boron in Zeolite for Oxidative Dehydrogenation of Propane. *Science* **2021**, *372*, 76−80.
(21) Lu, W.-D.; Wang, D.; Zhao, Z.; Song, W.; Li, W.-C.; Lu, A.-H. Supported Boron Oxide Catalysts for Selective and Low-Temperature Oxidative Dehydrogenation of Propane. *ACS Catal.* **2019**, *9*, 8263−8270.
(22) Tian, J.; Tan, J.; Xu, M.; Zhang, Z.; Wan, S.; Wang, S.; Lin, J.; Wang, Y. Propane Oxidative Dehydrogenation over Highly Selective Hexagonal Boron Nitride Catalysts: The Role of Oxidative Coupling of Methyl. *Sci. Adv.* **2019**, *5*, No. eaav8063.
(23) Love, A. M.; Cendejas, M. C.; Thomas, B.; McDermott, W. P.; Uchupalanun, P.; Kruszynski, C.; Burt, S. P.; Agbi, T.; Rossini, A. J.; Hermans, I. Synthesis and Characterization of Silica-Supported Boron Oxide Catalysts for the Oxidative Dehydrogenation of Propane. *J. Phys. Chem. C* **2019**, *123*, 27000−27011.
(24) Cendejas, M. C.; Dorn, R. W.; McDermott, W. P.; Lebrón-Rodríguez, E. A.; Mark, L. O.; Rossini, A. J.; Hermans, I. Controlled Grafting Synthesis of Silica-Supported Boron for Oxidative Dehydrogenation Catalysis. *J. Phys. Chem. C* **2021**, *125*, 12636−12649.
(25) Liu, Q.; Chen, C.; Liu, Q.; Wu, Y.; Xing, F.; Cheng, C.; Huang, C. Nonmetal Oxygen Vacancies Confined under Boron Nitride for Enhanced Oxidative Dehydrogenation of Propane to Propene. *Appl. Surf. Sci.* **2021**, *537*, 147927.
(26) Liu, Q.; Wu, Y.; Xing, F.; Liu, Q.; Guo, X.; Huang, C. B_2O_3@BPO_4 Sandwich-like Hollow Spheres as Metal-Free Supported Liquid-Phase Catalysts. *J. Catal.* **2020**, *381*, 599−607.
(27) Cao, L.; Dai, P.; Tang, J.; Li, D.; Chen, R.; Liu, D.; Gu, X.; Li, L.; Bando, Y.; Ok, Y. S.; Zhao, X.; Yamauchi, Y. Spherical Superstructure of Boron Nitride Nanosheets Derived from Boron-Containing Metal-Organic Frameworks. *J. Am. Chem. Soc.* **2020**, *142*, 8755−8762.
(28) Taylor, S. H.; Pollard, A. J. J. Silica and Boron Nitride Supported Molybdenum and Vanadium Oxide Catalysts for Propane Oxidation. *Catal. Today* **2003**, *81*, 179−188.
(29) Zhu, W.; Gao, X.; Li, Q.; Li, H.; Chao, Y.; Li, M.; Mahurin, S. M.; Li, H.; Zhu, H.; Dai, S. Controlled Gas Exfoliation of Boron Nitride into Few-Layered Nanosheets. *Angew. Chem., Int. Ed.* **2016**, *55*, 10766−10770.
(30) Kugai, J.; Miller, J. T.; Guo, N.; Song, C. Oxygen-enhanced water gas shift on ceria-supported Pd−Cu and Pt−Cu bimetallic catalysts. *J. Catal.* **2011**, *277*, 46−53.
(31) Shi, L.; Wang, D.; Song, W.; Shao, D.; Zhang, W.-P.; Lu, A.-H. Edge-Hydroxylated Boron Nitride for Oxidative Dehydrogenation of Propane to Propylene. *ChemCatChem* **2017**, *9*, 1788−1793.
(32) Zhang, Z.; Su, J.; Matias, A. S.; Gordon, M.; Liu, Y.-S.; Guo, J.; Song, C.; Dun, C.; Prendergast, D.; Somorjai, G. A.; Urban, J. J. Enhanced and Stabilized Hydrogen Production from Methanol by Ultrasmall Ni Nanoclusters Immobilized on Defect-Rich h-BN Nanosheets. *Proc. Natl. Acad. Sci. U.S.A.* **2020**, *117*, 29442−29452.
(33) Reich, S.; Ferrari, A. C.; Arenal, R.; Loiseau, A.; Bello, I.; Robertson, J. Resonant Raman Scattering in Cubic and Hexagonal Boron Nitride. *Phys. Rev. B: Condens. Matter Mater. Phys.* **2005**, *71*, 205201.
(34) Wu, Z.; Rondinone, A. J.; Ivanov, I. N.; Overbury, S. H. Structure of Vanadium Oxide Supported on Ceria by Multiwavelength Raman Spectroscopy. *J. Phys. Chem. C* **2011**, *115*, 25368−25378.
(35) Yan, H.; Alayoglu, S.; Wu, W.; Zhang, Y.; Weitz, E.; Stair, P. C.; Notestein, J. M. Identifying Boron Active Sites for the Oxidative Dehydrogenation of Propane. *ACS Catal.* **2021**, *11*, 9370−9376.
(36) Wilke, M.; Farges, F.; Petit, P.-E.; Brown, G. E.; Martin, F. Oxidation State and Coordination of Fe in Minerals: An Fe K-XANES Spectroscopic Study. *Am. Mineral.* **2001**, *86*, 714−730.
(37) Ressler, T.; Wong, J.; Roos, J.; Smith, I. L. Quantitative Speciation of Mn-Bearing Particulates Emitted from Autos Burning (Methylcyclopentadienyl)Manganese Tricarbonyl-Added Gasolines Using XANES Spectroscopy. *Environ. Sci. Technol.* **2000**, *34*, 950−958.
(38) Bañares, M. A.; Cardoso, J. H.; Hutchings, G. J.; Correa Bueno, J. M.; Fierro, J. L. G. Selective Oxidation of Methane to Methanol and Formaldehyde over V_2O_5/SiO_2 Catalysts. Role of NO in the Gas Phase. *Catal. Lett.* **1998**, *56*, 149−153.
(39) Zalc, J. M.; Green, W. H.; Iglesia, E. NO_x-Mediated Homogeneous Pathways for the Synthesis of Formaldehyde from CH_4-O_2 Mixtures. *Ind. Eng. Chem. Res.* **2006**, *45*, 2677−2688.
(40) Annamalai, L.; Liu, Y.; Deshlahra, P. Selective C−H Bond Activation via NO_x-Mediated Generation of Strong H-Abstractors. *ACS Catal.* **2019**, *9*, 10324−10338.
(41) Gouin, X.; Grange, P.; Bois, L.; L'Haridon, P.; Laurent, Y. Characterization of the Nitridation Process of Boric Acid. *J. Alloys Compd.* **1995**, *224*, 22−28.
(42) Wang, Y.; Trenary, M. Surface Chemistry of Boron Oxidation. 2. The Reactions of Boron Oxides B_2O_2 and B_2O_3 with Boron Films Grown on Tantalum(110). *Chem. Mater.* **2002**, *5*, 199−205.

https://doi.org/10.1021/jacsau.1c00542
JACS Au 2022, 2, 1096−1104